Enhanced climate variability during the last millennium recorded in alkenone sea surface temperatures of the northwest Pacific margin

Kyung Eun Lee[1,2*], Wonsun Park[3], Sang-Wook Yeh[4], Si Woong Bae[2], Tae Wook Ko[2], Gerrit Lohmann[5], Seung-Il Nam[6]

[1] Department of Ocean Science, Korea Maritime and Ocean University, South Korea

[2] Ocean Science and Technology School, Korea Maritime and Ocean University, South Korea

[3] GEOMAR Helmholtz Centre for Ocean Research Kiel, 24105 Kiel, Germany

[4] Department of Marine Science and Convergence Engineering, Hanyang University, ERICA, 15588, South Korea

[5]Alfred-Wegener-Institute, Bremerhaven 27570, Germany

[6] Arctic Research Center, Korea Polar Research Institute, Incheon, South Korea

[*] Corresponding author:
Email address: kyung@kmou.ac.kr (Kyung Eun Lee)

June 17, 2021

For reresubmission to *Global and Planetary Change*

Abstract

Previous studies on surface temperature reconstructions for the last 2,000 years (2k) revealed a long-term cooling trend for the last millennium in comparison to the previous millennium. However, knowledge on the decadal- to centennial-scale variability in sea surface temperature and the underlying governing mechanisms throughout the period is limited. We reconstructed high-resolution continuous sea surface temperature changes over the last 2k in the northwest Pacific margin based on the alkenone unsaturation index. Our alkenone temperature record revealed enhanced and more rapidly changing climate variability during the last millennium (approximately 1200–1850 Common Era) than during the previous millennium. Cold and hot extremes also occurred more frequently during the last millennium. The enhanced and rapidly changing climate variability appears to be associated with frequent volcanic eruptions and grand solar minima. The reconstructed surface temperature variability tends to be associated with variations in the East Asia summer monsoon and the Pacific Decadal Oscillation, implying that these variations are also enhanced in the last millennium than in the previous millennium.

Keywords: last millennium, Common Era, past sea surface temperature, volcanic forcing, East Asian summer monsoon, North Pacific

1. Introduction

The network of the Past Global Changes project synthesised surface temperature data for the past 2,000 years (herein 2k) to reconstruct regional and global variations (PAGES 2k Consortium, 2013). All of the continental temperature records compiled display a long-term cooling trend beginning at approximately 1200 CE and ending in the nineteenth century, although these past global changes exhibited strong regional differences in timing of cooling (PAGES 2k Consortium, 2013). A global synthesis of sea surface temperatures (SST) also revealed a cooling trend that began earlier and was sustained for a millennium (801–1800 CE) (McGregor *et al.*, 2015). However,

due to the issues of scarcity, resolution, continuity, and uncertainty of the SST records, they provided only the 200-year averaged data. Therefore, it was difficult to identify the multi-decadal- and centennial-scale variations in SST over the last 2k from the records. Even today, a scarcity of high-resolution SST records over the last 2k impedes further progress toward identifying the natural variability itself on multi-decadal and centennial scales, and understanding the relations with climate forcing.

Previous studies on data reconstruction and model simulations tried to identify internal and external forcing associated with the reconstructed temperature variations including parameters of solar irradiance, volcanic activity, land-cover changes, and orbital-driven insolation, and the results suggested that the cooling trend of the ocean surface temperature over the period of 801–1800 CE was not primarily a response to solar forcing but may have been related to the increased frequency of explosive volcanism (McGregor *et al.*, 2015). Recently, Atlantic multi-decadal variability over the past 1,200 years was clarified using terrestrial proxy records from the circum-North Atlantic region (Wang *et al.*, 2017) and the results suggested that natural external forcing (volcanic and solar irradiation) explained approximately 30% of the variance observed in the reconstruction on multi-decadal scale, and that internal dynamic processes may have played a role in the variations instead. In addition, the reconstruction of changes in SST off the coast of Baja California in the eastern subtropical Pacific during the last 2k revealed discontinuous multi-decadal variability with periodicities similar to instrumental observations of the Pacific Decadal Oscillation (PDO) and a relationship with megadroughts in southwestern North America (O'mara *et al.*, 2019).

To improve our understanding of climate variability, SST reconstruction from the marine paleoclimate archive is essential, but SST data in the western margin of the North Pacific is still lacking. In this study, we examine the extent to which the natural variability in surface temperature has changed over the past 2k. Instrumental climate

records are available only for the last 100 years. In particular, continuous high-resolution SST records prior to the last century are very limited. To overcome this issue, new SST records covering the past 2k were reconstructed using the marine sediments near the Korean Peninsula. Quantification of past SST changes at high resolution can be used to identify climate variability on multi-decadal and centennial timescales over the past 2k. Furthermore, the comparisons of the record with climate forcing and other paleoclimatic records, including the East Asian monsoon and SST records from other regions, help to understand relations between major variability in climate system over the past 2k.

Paleotemperature reconstruction by alkenones is based on the widely accepted hypothesis that haptophyte microalgae produce long chain (C_{37}) alkenones, whose degree of unsaturation changes with seawater temperature. The relationship between the alkenone unsaturation index ($U^{K'}_{37}$) and the temperature of seawaters in which the algae grow has been calibrated using results from laboratory culture experiments involving *Emiliania huxleyi* (e.g. Prahl and Wakeham, 1987; Prahl *et al*., 1988), and from the results of analysis of surface water and sediments trap samples (e.g. Prahl *et al*., 1993), and coretop sediment samples (e.g. Müller *et al*., 1998). In particular, a bi-monthly record of total C_{37} alkenone concentrations measured from suspended particles in surface waters near the Korean Peninsula (Lee *et al*., 2014) confirmed that the calibration equation given by Prahl *et al*. (1988; $U^{K'}_{37}=0.034T + 0.039$) is applicable in this area. In this study, we reconstructed alkenone SST variations from marine sediments with a higher temporal resolution of approximately 2–8 years, constituting the first well-preserved, long, and continuous SST record of the northwestern Pacific margin spanning the past 2k. The record reveals the characteristics of temporal variations in temperature in the region on multi-decadal to centennial timescales, although age uncertainty should be considered.

2. Materials and methods

Bi-monthly SSTs observed *in situ* at the study area over the period of 2000–2012 were collected from a National Fisheries Research and Development Institute (NFRDI) dataset (Fig. 1). The seasonal SST variations were large (13–24 °C) in the study area. Sea surface salinity ranged from 32.2 psu in summer to 34.4 psu in winter according to the NFRDI dataset. Lower salinity occurred in summer, which was due to dilution by summer monsoon river discharge from the adjacent drainage basins of the Korean peninsula and China including the Yangtze River.

A piston core, TY2010 PC4, was collected from a shelf mud deposit off the east coast of the Korean Peninsula during a R/V Tamyang cruise in 2010. The core was 3.44 m long, and was located at the northern part (129°36'E, 35°50'N) of the mud deposit at a water depth of 91 m. A gravity core (ARA/ES 03-01 GC01, 5.45 m in length) was obtained from the same site as that of core TY2010 PC4 during a R/V Araon cruise in 2012. Lithologies and X-ray radiographs of both cores indicated that the marine sediments predominately consist of hemipelagic mud. Because the ARA/ES 03-01 GC01 core contains the longer proxy record, we primarily used this core. However, for the upper section (~1 m), the piston core was used instead. This avoided the potential loss of the upper portion of the sediment that is more likely to occur when using the gravity coring method (e.g. Skinner and McCave, 2003).

Bulk sediment samples (3 g) were taken from the TY2010 PC4 core at 2-cm intervals for alkenone analysis. For the ARA/ES 03-01 GC01 core, the samples were collected at 2-cm intervals in the upper part of the core (0–340 cm) and at 1-cm intervals in the lower part (340–545 cm). The alkenone analysis was conducted at the Korea Maritime and Ocean University. C_{37} alkenones were extracted from the freeze-dried sediment samples. Organic compounds were extracted using an ASE-200 solvent extractor (Dionex Corporation) with a solvent mixture (CH_2Cl_2:CH_3OH, 99:1 v/v) at a high temperature (100 °C) and pressure (1500 psi). The extracts were cleaned via elution with 3 × 500 μL CH_2Cl_2 through a commercial silica cartridge. Saponification

was performed at 70 °C for 2 h with 0.1 M KOH. The neutral fraction containing the alkenones was obtained by partitioning into hexane. After being concentrated under N_2, the final extract was analysed by gas chromatography with an Agilent 7890A chromatograph equipped with a flame ionisation detector and fused-silica capillary column (J&W DB-1, 60 m × 0.32 mm). The alkenone temperatures were calculated using the alkenone unsaturation index ($U^{K'}_{37}=[C_{37:2}] / ([C_{37:2}]+[C_{37:3}])$) and the calibration equation given by Prahl *et al*. (1988; $U^{K'}_{37}=0.034T + 0.039$). A new calibration, BAYSPLINE (Tierney and Tingley, 2018), was also applied to calculate seawater temperatures from the $U^{K'}_{37}$ values. BAYSPILNE produced the exact same SST estimates as those produced using the calibration method of Prahl *et al*. The reproducibility of the alkenone temperatures for replicate samples of a homogeneous marine sediment laboratory standard run during this project was better than ± 0.1 °C (n = 27, 1σ). Duplicate analyses on ARA/ES 03-01 GC01 gave results within ± 0.2 °C (n = 50, 1σ).

The ARA/ES 03-01 GC01 core ages were determined via radiocarbon dating (Table 1 and Fig. 2). Accelerator mass spectrometry (AMS) ^{14}C dates of planktonic foraminifera were measured at the Rafter Radiocarbon Laboratory, New Zealand (at two depths) and the National Ocean Sciences AMS (NOSAMS) facility at the Woods Hole Oceanographic Institution (WHOI), USA (at six depths). Although the dates were measured by two different institutes, the results were extremely consistent. An age-depth model was constructed using the Bacon 2.2 package in R (Blaauw and Christen, 2011) (Fig. 2). Bacon simulates the accumulation rates of core sediments based on Bayesian statistics and calculates the ages and uncertainties (1σ) of sediment deposits. The results of the ^{210}Pb dating of the box core NR2018 BC2 sediments (129°35.4'E, 35°52'N) collected near the ARA/ES 03-01 GC01 core are presented in Table 2. The ^{210}Pb and ^{226}Ra activities were measured at the Korea Basic Science Institute (KBSI). The observed excess ^{210}Pb activities in the NR2018 BC2 core indicate that the core-top surface sediments are modern-day sediments.

The study area is characterised by an extremely high sedimentation rate of approximately 0.5 cm/yr, making the site ideal for a high-resolution study of past surface temperature changes. The entire core covers the last 1,900 years (Fig. 2). However, the variability in accumulation rate of the core indicates a distinctive change in accumulation rate at a depth of 340 cm, corresponding to the year 1453 CE (Fig. 2). The mean value of the accumulation rate was 1–2 yr/cm (±1.8–3, 1σ) after 1453 CE, whereas it was 4–8 yr/cm (±6–13, 1σ) before 1453 CE. Hence, the sedimentation rates are different, at approximately 1–0.5 cm/yr for the upper part of the core and 0.1 cm/yr for the lower part. Alkenone temperature resolution is approximately 2–4 years for the upper part and 6–8 years for the lower part. The Bayesian statistics-based age-depth model indicates that the uncertainties in the ages of sediments younger than 1453 CE are relatively small (±10–20 yr), while the uncertainties in the ages of older sediments are large (±16-40 yr) (top panel in Fig. 3).

For comparisons of alkenone SST recod with other paleoclimatic records, we calculate correlation coefficients between them by using the Ebisuzaki method which is suitable for a serial correlation analysis. This method was conducted by implementing the 'surrogateCor' function in the R package 'astrochron' (Ebisuzaki, 1997, Meyers, 2014, Baddouh *et al*., 2016) with 10,000 Monte Carlo simulations.

3. Results

A new high-resolution alkenone SST record for the last 2k was constructed by combining records from cores TY2010 PC4 and ARA/ES 03-01 GC01. The core-top temperature estimated from the $U^{K'}_{37}$ value was 20.5 °C. A comparison with the 12-year averaged SSTs measured *in situ* (2000–2012) showed that the core-top alkenone temperature is higher than the observed annual mean SST (17.7 °C), and that it is close to the observed temperatures in June to October (Fig. 1). A bi-monthly record of total C_{37} alkenone concentrations measured from suspended particles in surface

196 waters at the core site shows that the concentration is the highest during summer (Fig.
197 1), indicating that the alkenones are predominantly produced in summer (Lee *et al*.,
198 2014). In addition, alkenone analysis of the subsurface samples from the *in situ* bottle
199 casts show that the concentration of total C_{37} alkenones was typically high in the
200 surface mixed layer and decreased with depth, indicating that alkenones were most
201 likely produced in the surface mixed layer and thus that alkenone records from marine
202 sediments represent near-surface signals (Lee *et al*., 2014).
203
204 Temporal variations in alkenone SSTs exhibited millennial evolution and fluctuations
205 on multi-decadal to centennial timescales during the last 2k (Fig. 3a). The increase in
206 temperature since the mid-19th century is clear, which is associated with an
207 anthropogenically induced global warming trend (IPCC, 2013). During the first of the
208 two millennia, alkenone temperatures fluctuated between 19.4 °C and 21 °C. A cooler
209 period occurred between 850 CE and 1200 CE. Hence, the Medieval Climate
210 Anomaly interval (approximately 950–1250 CE) is not reflected clearly in this record.
211 During the last millennium, there were several pronounced cold periods (e.g. 1267–
212 1280 CE and 1626–1629 CE), and a few strong cooling events were centred at around
213 1715 CE, 1820 CE, and 1910 CE. The lowest temperature (18.7 °C) occurred in
214 approximately 1267±28 CE. Comparisons of alkenone temperatures with tree-ring-
215 based temperature records from the Korean Peninsula for the period of 1640–1989 CE
216 (Choi *et al*., 1992) revealed that the cooling events identified from the tree ring data at
217 1690 CE, 1730 CE, 1840 CE, and 1910 CE are consistent with those identified in the
218 alkenone temperature records. Our SST record was also compared to tree ring-based
219 air temperatures in Asia (PAGES 2k Consortium, 2013). A long-term cooling trend in
220 the synthesised surface temperature in Asia beginning in approximately 1200 CE is
221 consistent with that of our SST record (Fig. 3a and c).
222
223 Our record reveals that climate variability increased during the last millennium,
224 especially in the period of 1200–1850 CE, relative to the preceding period of 500–

225 1200 CE. SST variations range within ~3 °C over the period of 1200–1850 CE and
226 ~1 °C over 500–1200 CE (Fig. 3a). In this study, we used 10-year averaged SST for
227 the entire period of the last 2k to overcome the issue of time resolution of the record.
228 It should be noted that even though the record for the last millennium is smoothed so
229 as to emulate the resolution of the record for the first millennium, the increased
230 variability in SST is still identified for the last millennium. During the period of
231 1200–1850 CE, cold and hot extremes (deviations of over 1σ) were more frequent.
232 The magnitude of the running standard deviation (100-year window) was larger over
233 1200–1850 CE than over the earlier period (Fig. 3b). We investigated changes in the
234 accumulation rate to ascertain whether the enhanced and rapid climate changes were
235 associated with the sediment deposition rate. The accumulation rate of the upper part
236 of the core (1–2 yr/cm after 1453 CE) was different from that of the lower part (4–8
237 yr/cm). We do not exclude the possibility that the enhanced variability in the alkenone
238 SST of the upper part of the core is related to changes in the accumulation rate.
239 However, the greatest variability in the SST running standard deviation occurred over
240 1200–1450 CE, which corresponds to a period of low sedimentation rates. The lowest
241 temperature also occurred during this interval. These results indicate that the
242 enhanced and rapid climate changes were not simply due to an increase in
243 sedimentation rate. This suggests that, although the alkenone SST variability of the
244 lower part of the core can be smoothed to some extent due to the low sedimentation
245 rate, cold events and rapid climate changes are still recognisable.
246
247 We compared our alkenone temperature record to records of solar irradiation and
248 volcanic activity covering the last 2k to examine the extent to which alkenone SST
249 changes are correlated with changes in these phenomena (Fig. 4a, b, c). The total solar
250 irradiation (TSI) data for the last 2k used in the study were reconstructed based on
251 radiocarbon production and solar activity instrumental data (Roth and Joos, 2013).
252 According to the record, the overall solar irradiance for the first millennium of this
253 period was stronger than that of the last millennium. Four distinct grand solar minima

known as the Oort (1040–1080 CE), Wolf (1280–1350 CE), Maunder (1645–1715 CE), and Dalton (1790–1820 CE) were identified within the last millennium (Steinhilber and Beer, 2011). The minima appear to be correlated with the cold alkenone temperatures of the study area, considering the age uncertainty (Fig. 4b and c). However, variations in TSI did not always coincide with variations in alkenone SST, such as during the Spoerer period (1460–1550 CE) (Fig. 4b and c). In addition, the minimum in the temperature record apparently precedes the minimum in solar activity (Fig. 4b and c). Spectrum analysis was performed on both time series of alkenone temperature and TSI for the last 2k. There are discrepancies in the periodicity of spectral peaks between the two time series (Fig. 5). However, at centennial time scale, significant peaks in the SST record are 94-year and 80-year, and those in TSI are 106-year and 89-year, respectively (Fig. 5). There might be some coherence between them (94-year and 80-year versus 106-year and 89-year). The differences are within the range of ±10%. This may indicate that the solar forcing influence on the SST variability considering the uncertainty in each dataset. We also calculated the correlation coefficient between the reconstructed SST and the TSI (Table 3). The correlation is not significant for the entire period, but it becomes large (0.54 at 99% confidence level) when the period is confined to the last 400 years (1600-2000 CE). Although the correlation coefficient does not imply the causality, this result may indicate that the variability of solar forcing plays a role on the SST variability. However, in general, solar activity seems to be insufficient for explaining the entire SST cooling trend.

Previous studies have suggested that volcanic eruptions played an important role in climate variations (Sigl *et al*., 2015). The record of volcanic activity over the last 2k was reconstructed based on atmospheric aerosol loading as measured in ice cores (Sigl *et al*., 2015). Comparisons of our SST temperature record with the atmospheric aerosol forcing record demonstrated that episodic cooling events identified in our record match with the volcanic activity record in terms of intensity and frequency

283 within the error range of age determination (Fig. 4a and b). Overall, the magnitude of
284 volcanic forcing ranges 8-12 W/m^2 for the first millennium, and 8-15 W/m^2 with the
285 maximum of 32 W/m^2 for the second millennium (Fig. 6a). In addition, the number of
286 occurrence of volcanic eruption significantly increased from the first to the second
287 millennium (Fig. 6b). These imply that the volcanic forcing may significantly
288 contribute to influence the enhanced SST variability during the second millennium.
289 On the other hand, changes in total solar irradiance range less than ~1 W/m^2 over the
290 last 2k (Fig. 6c). Hence, the impact of volcanic forcing on surface temperature would
291 be greater than that of solar insolation forcing. In particular, a tropical volcanic
292 eruption in 1258 CE (Samalas Volcano, Indonesia) (Lavigne *et al*., 2013) correlated
293 with an event-like cooling observed in our record. Although the Bayesian statistics-
294 based age-depth model indicated an age uncertainty of ±28 yr for the period of 1267–
295 1280 CE, the timing of the cooling event is consistent with that of the volcanic
296 activity. Furthermore, the increased frequency of volcanic events over the interval of
297 1258–1286 CE may be related to abnormally strong cooling during the time period,
298 indicating a large contribution of volcanic activity toward climate changes. These
299 observations are consistent with previous results, demonstrating that strong and
300 frequent volcanic eruptions in the tropics and at high latitudes could have been
301 primary drivers of interannual to decadal temperature variability in the Northern
302 Hemisphere throughout the past 2k (Sigl *et al*., 2015).
303
304 It is also noteworthy that Earth system model simulations indicate the surface cooling
305 of East Asia in summer after large volcanic eruptions (Man *et al*., 2014). According to
306 these simulations, the cooling appeared to be proportional to the magnitude of the
307 volcanic forcing, and it persisted for a few years after some of the largest eruptive
308 episodes. The cooling in 1258 CE could have begun in connection with volcanic
309 activity, and it lasted several decades in connection with the Wolf solar minimum.
310 Hence, the enhanced climate variability becomes evident when a volcanic forcing is
311 accompanied by grand solar minimum and the occurrence of volcanic eruption

312 increases for the time period. In contrast, the reconstruction of greenhouse gas (CO_2,
313 CH_4, and N_2O) forcing levels from ice core data (MacFarling Meure *et al*., 2006; Joos
314 and Spahni, 2008) showed that the response of SST to greenhouse gas forcing seemed
315 to be less significant during this time period (Fig. 4d).
316
317 **4. Discussion**
318 Our alkenone SST record was obtained from one location in the northwestern
319 subtropical Pacific margin. To examine how this record may represent a regional SST
320 pattern, the alkenone SST data were compared with instrumental datasets including
321 extended-reconstructed SST (ERSST v4, Huang *et al*., 2014) and the Hadley Centre
322 Sea Ice and SST dataset (HadISST, Rayner *et al*. 2003) for 1870-2010. Figure 7a
323 shows the time series of the alkenone SST along with the averaged SST over June to
324 October from the ERSSTv4 and HadISST datasets covering the past 140 years. It was
325 found that the records are comparable with one another. To further examine the
326 regional SST pattern associated with the alkenone SST record, we calculated
327 regressed SST anomalies against the alkenone temperature by using the 11-year
328 running mean SST of the HadISST dataset, since the age resolution of the alkenone
329 temperature and the timescale of interest are greater than one year. The regression
330 map of HadISST and alkenone temperatures (Fig. 7b) shows that the correlation with
331 local SST is strong. The regressed SST anomalies against alkenone temperatures were
332 characterised by a relatively good relationship along the subtropical western boundary
333 current in the North Pacific. This indicates that SST changes identified at our study
334 site are representative of those of the North Pacific Ocean basin and the Kuroshio and
335 the Kuroshio extension in particular. We also constructed the regression by using
336 detrended SST to eliminate a global warming trend that would have dominated the
337 spatial pattern over the last 140 years. The detrended SST regression pattern shown in
338 Fig. 7c displays the PDO-like pattern, which is characterised by cooling in the central
339 North Pacific and warming along the west coast of the USA (Mantua and Hare, 2002).
340 This result indicates that the variability in SST at the core site tended to coincide with

that of a PDO-like SST pattern and the PDO-like SST variability is enhanced in the last millennium than in the previous millennium.

A recently published alkenone SST record for the last 2k of the eastern subtropical Pacific captures multi-decadal variations that may relate to the PDO (O'Mara *et al.*, 2019). The alkenone temperature anomalies shown in Fig. 8a and b were constructed based on the 10-year averaged temperatures in consideration of the difference in data resolution bewteen the first and the second millennia. The correlation coefficient and statistical probability between our alkenone SSTs and those of O'Mara et al. (2019) for the last 2k were calculated. It was difficult to present statistically meaningful correlations for the last 2k. This is probably either because the PDO pattern is not stationary, or because the age uncertainty is large. However, there seem to be opposite temperature patterns on the multi-decadal and centennial time scales. For examples, for the intervals centred at 500 CE and 750 CE, the western Pacific region was relatively warm, while the eastern Pacific region predominantly cooled. During the period of 1600-1700 CE, it was cold in the west, and warm in the east. Since 1800 CE, warming has been dominant in the west, and cooling has dominated in the east. In addition, the running standard deviation patterns of both alkenone records for a 100-year sliding window were consistent for the last millennium (Fig. 8c), indicating that both records contain enhanced multi-decadal to centennial variations during the period of 1200–1850 CE.

In this study, changes in the reconstructed SST were compared to the evolution of the East Asian summer monsoon system over the last 2k (Fig. 9). Recent studies on variability in the East Asia summer monsoon (EASM) (Chiang et al., 2017, Liu et al., 2014, Zhang *et al*., 2018) showed that the EASM system undergoes complex spatio-temporal evolution. For example, the variability of a tripole mode of rainfall anomalies, which is characterised by a drier central-to-eastern China and a wetter southern and northern China, is dominant in East Asia during the boreal summer on

an interannual timescale. When the rainfall anomalies from NOAA dataset (Chen et al., 2002) were statistically regressed against the instrumental SST (i.e. HadISST) of our study area over the last 71 years, the tripole mode pattern was also exhibited (Fig. 9a). In general, Chinese cave $\delta^{18}O$ signals reflect regional rainfall in East Asia, where higher EASM rainfall corresponds to more-depleted $\delta^{18}O$ (e.g. Cheng *et al*., 2009). Time series of 10-year averaged alkenone temperature and Chinese cave $\delta^{18}O$ records for the last 2k were compared with each other. The Wanxiang stalagmite $\delta^{18}O$ record from near the upper Yangtze River (Zhang *et al.*, 2008) contains light values (corresponding to increased rainfall) for the periods of 400–700 CE and heavy values (decreased rainfall/drought) for the period of 1300–1800 CE (Fig. 9b). The correlation coefficient between our SST record and the cave monsoon record for the period of 1200-1850 CE is significantly high ($r = -0.34$, $P = 0.003$). On the other hand, the stalagmite $\delta^{18}O$ record from Dongge cave (Wang *et al*., 2005), located in South China, exhibits heavy values (decreased rainfall/drought) for the periods of 400–700 CE and less-heavy and light values (increased rainfall) for the periods of 1400-1600 CE and 1700-1900 CE, respectively (Fig. 9e). Hence, the rainfall/drought patterns of the Wanxiang and Dongge are in opposition. The stalagmite $\delta^{18}O$ record from Shenqi cave (Tan *et al*., 2018) shows a pattern different from that of the Wanxiang record, as indicated by the correlation coefficient ($r = 0.4$, $p = 0.03$) (Fig. 9c). The record from Heshang cave (Hu *et al*., 2008) does not show a clear pattern (Fig. 9d). The complicated patterns exhibited in the stalagmite $\delta^{18}O$ records seem to be associated with variations in the tripole mode of the EASM-related rainfall in China, given that the cave $\delta^{18}O$ records indicate regional rainfall.

For the period of 400-700 CE, EASM-related precipitation increased, and pluvials may have dominated near the upper Yangtze River. The light values given in the Wanxiang stalagmite $\delta^{18}O$ record support this theory. Relatively warm SSTs at our core site appear to also be correlated with this pattern. However, southern China experienced drought in this period. For the period of 1400-1600 CE, drought

399 prevailed across China (Cook *et al.*, 2010), which is also supported by all cave
400 records. Severe drought near the upper Yangtze River around 1600-1700 CE was
401 linked to strong cooling at our core site. A seawater $\delta^{18}O$ record covering 1,300 years
402 that was reconstructed using foraminiferal $\delta^{18}O$ and alkenone temperature data from
403 near our core site displayed a pattern similar to that of the Wanxiang stalagmite $\delta^{18}O$
404 record (Lee and Park, 2015). It is noteworthy that the rainfall increased in the south of
405 China in the period of 1700-1900 CE, as indicated by the Dongge stalagmite $\delta^{18}O$
406 record. The alkenone SST in our record increased in the same period. Overall,
407 Chinese cave $\delta^{18}O$ records revealed increased multi-decadal to centennial variability
408 during the last millennium in comparison to that in the previous millennium.
409
410 **5. Summary**
411 The first well-preserved, high-resolution, continuous SST record of the northwestern
412 Pacific margin spanning the past 2k revealed enhanced and rapid climate variability
413 on multi-decadal to centennial timescales in the last millennium, which differed
414 significantly from that in the previous millennium. A comparison of the SST record
415 with volcanic and solar insolation records suggested that the enhanced variability in
416 surface temperature was associated with changes in these phenomena, such as
417 increased volcanic activity and grand solar minima during this period, implying that
418 natural variability in these factors plays a role in increased regional climate variability.
419 In addition, the reconstructed SST record at the core site represents the PDO-like
420 variability, which is also enhanced in the last millennium than in the previous
421 millennium. Comparisons of the SST record with $\delta^{18}O$ records of Chinese caves
422 revealed correlations between temperatures and the monsoon system over the past 2k,
423 suggesting that surface temperature extremes seem to be related to monsoon activity
424 and hydrological cycle reinforcement in the upper Yangtze River with greater
425 variability during the last millennium in comparison to that in the previous
426 millennium.
427
428

Acknowledgements

We thank reviewers and the Editor for their constructive comments and suggestions. This work was supported by a National Research Foundation of Korea grant funded by the South Korean government (Ministry of Science and ICT) (grant no. 2019R1A2C2004951) awarded to K.E. Lee. Paleoclimate proxy data relevant to this study are attached as Supplementary Information. Correspondence should be addressed to K.E. Lee.

438 **References**

439 Baddouh, M., Meyers, S.R., Carroll, A.R., Beard, B.L., Johnson, C.M., 2016.
440 Lacustrine $^{87}Sr/^{86}Sr$ as a tracer to reconstruct Milankovitch forcing of the Eocene
441 hydro-logic cycle. Earth Planet. Sci. Lett. 448, 62–68.

442 Blaauw, M., Christen, J.A., 2011. Flexible paleoclimate age-depth models using an
443 autoregressive gamma process. Bayesian Anal. 6(3), 457–474.

444 Cheng, H., Edwards, R.L., Broecker, W.S., Denton, G.H., Kong, X., Wang, Y., Zhang,
445 R., Wang X., 2009. Ice age terminations. Science 326, 248-252.

446 Chiang, J.C.H.. Swenson, L.M., Kong, W., 2017, Role of seasonal transitions and the
447 westerlies in the interannual variability of the East Asian summer monsoon
448 precipitation. Geophys. Res. Lett. 44, 3788-3795.

449 Chen, M., P. Xie, J. E. Janowiak, and P. A. Arkin, 2002: Global Land Precipitation: A
450 50-yr Monthly Analysis Based on Gauge Observations, J. of Hydrometeorology,
451 3, 249-266.

452 Choi, J.N., Yu, K.B., Park, W.K., 1992. Paleoclimate reconstruction for Chungbu
453 mountainous region using tree-ring chronology. Korean J. Quat. Res. 6(1), 21–32.
454 (in Korean with English abstract)

455 Cook, E.R., Anchukaitis, K.J., Buckley, B.M., D'Arrigo, R.D., Jacoby, G.C., Wright,
456 W.E., 2010. Asian monsoon failure and megadrought during the last millennium.
457 Science 328, 486–489.

458 Ebisuzaki, W., 1997. A method to estimate the statistical significance of a correlation
459 when the data are serially correlated. J. Clim. 10, 2147–2153.

460 Hu, C., Henderson, G.M., Huang, J., Xie, S., Sun, Y., Johnson, K.R., 2008.
461 Quantification of Holocene Asian monsoon rainfall from spatially separated cave
462 records. Earth planet. Sci. lett 266, 221-232. Doi: 10.1016/j.epsl.2007.10.015.

463 Huang, B., Banzon, V.F., Freeman, E., Lawrimore, J., Liu, W., Peterson, T.C., Smith,
464 T.M., Thorne, P.W., Woodruff, S.D., Zhang, H.-M., 2014: Extended
465 Reconstructed Sea Surface Temperature version 4 (ERSST.v4): Part I. Upgrades
466 and intercomparisons. *Journal of Climate*, **28**, 911–930.

IPCC, 2013. Climate Change 2013: The Physical Science Basis. Contribution of Working Group I to the Fifth Assessment Report of the Intergovernmental Panel on Climate Change [Stocker, T.F., D. Qin, G.-K. Plattner, M. Tignor, S.K. Allen, J. Boschung, A. Nauels, Y. Xia, V. Bex and P.M. Midgley (eds.)]. Cambridge Univ. Press, Cambridge, United Kingdom and New York, NY, USA, 1535 pp.

Joos, F., Spahni, R., 2008. Rates of change in natural and anthropogenic radiative forcing over the past 20,000 years. Proc. Natl. Acad. Sci. 105, 1425–1430.

Lavigne, F., Degeai, J.-P., Komorowski, J.-C., Guillet, S., Robert, V., Lahitte, P., Oppenheimer, C., Stoffel, M., Vidal, C.M., Surono, Pratomo, I., Wassmer, P., Hajdas, I., Hadmoko, D.S., de Belizal, E., 2013. Source of the great A.D. 1257 mystery eruption unveiled, Samalas volcano, Rinjani Volcanic Complex, Indonesia. Proc. Natl. Acad. Sci. 110, 16742-16747.

Lee, K.E., Lee, S., Park, Y., Lee, H.J., Harada, N., 2014. Alkenone production in the East Sea/Japan Sea. Cont. Shelf Res. 74, 1-10.

Lee, K.E., Park, W., 2015. Initiation of East Asia monsoon failure at the climate transition from the Medieval Climate Anomaly to the Little Ice Age. Glob. Planet. Chang. 128, 83-89.

Liu, Z., Wen, X., Brady, E.C., Otto-Bliesner, B., Yu, G., Lu, H., Cheng, H., Wang, Y., Zheng, W., Ding, Y., Edwards, R.L., Cheng, J., Liu, W., Yang, H., 2014. Chinese cave records and the East Asia Summer Monsoon. Quat. Sci. Rev. 83, 115-128. doi:10.1016/j.quascirev.2013.10.021

MacFarling Meure, C., Etheridge, D., Trudinger, C., Steele, P., Langenfelds, R., van Ommen, T., Smith, A., Elkins, J., 2006. Law Dome CO_2, CH_4 and N_2O ice core records extended to 2000 years BP. Geophys. Res. Lett. 33, L14810.

Man, W., Zhou, T., Jungclaus, J.H., 2014. Effects of large volcanic eruptions on global summer climate and East Asian monsoon changes during the last millennium: analysis of MPI-ESM simulations. J. Clim. 27, 7394-7409.

Mantua, N.J., Hare, S.R., 2002. The Pacific Decadal Oscillation. J. Oceanogr. 58, 35-44.

McGregor, H.V., Evans, M.N., Goosse, H., Leduc, G., Martrat, B., Addison, J.A., Mortyn, P.G., Oppo, D.W., Seidenkrantz, M.-S., Sicre, M.-A., Phipps, S.J., Selvaraj, K., Thirumalai, K., Filipsson, H.L., Ersek, V., 2015. Robust global ocean cooling trend for the pre-industrial Common Era. Nat. Geosci. 8, 671-677.

Meyers, S.R., 2014. Astrochron: An R Package for Astrochronology. https://cran.r-project.org/package=astrochron.

Müller, P.J., Kirst, G., Ruhland, G., von Storch, I., Rosell-Melé, A., 1998. Calibration of the alkenone paleotemperature index $U_{37}^{K'}$ based on core-tops from the eastern South Atlantic and the global ocean (60°N-60°S). Geochim. Cosmochim. Acta 62, 1757-1772.

O'Mara, N.A., Cheung, A.H., Kelly, C.S., Sandwick, S., Herbert, T.D., Russell, J.M., Abella-Gutiérrez, J., Dee, S.G., Swarzenski, P.W., Herguera, J.C., 2019. Subtropical Pacific Ocean temperature fluctuations in the Common Era: multidecadal variability and its relationship with Southwestern North American Megadroughts. Geophys. Res. Lett. 46, https://doi.org/10.1029/2019GL084828.

PAGES 2k Consortium, 2013. Continental-scale temperature variability during the past two millennia. Nat. Geosci. 6, 339-346.

Prahl, F.G., Wakeham, S.G., 1987. Calibration of unsaturation patterns in long-chain ketone compositions for palaeotemperature assessment. Nature 330, 367-369.

Prahl, F.G., Muehlhausen, L.A., Zahnle, D.L., 1988. Further evaluation of long-chain alkenones as indicators of paleoceanographic conditions. Geochim. Cosmochim. Acta 52, 2303–2310.

Prahl, F.G., Collier, R.B., Dymond, J., Lyle, M., Sparrow, M.A.,1993. A biomarker perspective on prymnesiophyte productivity in the northeas Pacific Ocean. Deep-sea Res. 40, 2061-2076.

Rayner, N.A., Parker, D.E., Horton, E.B., Folland, C.K., Alexander, L.V., Rowell, D.P., Kent, E.C., Kaplan, A., 2003. Global analyses of sea surface temperature, sea ice, and night marine air temperature since the late nineteenth century. J. Geophys. Res. 108, 4407.

525 Roth, R., Joos, F., 2013. A reconstruction of radiocarbon production and total solar
526 irradiance from the Holocene ^{14}C and CO_2 records: implications of data and
527 model uncertainties. Clim. Past 9, 1879-1909.
528 Sigl, M., Winstrup, M., McConnell, J.R., Welten, K.C., Plunkett, G., Ludlow, F.,
529 Büntgen, U., Caffee, M., Chellman, N., Dahl-Jensen, D., Fischer, H., Kipfstuhl,
530 S., Kostick, C., Maselli, O.J., Mekhaldi, F., Mulvaney, R., Muscheler, R., Pasteris,
531 D.R., Pilcher, J.R., Salzer, M., Schüpbach, S., Steffensen, J.P., Vinther, B.M.,
532 Woodruff, T.E., 2015. Timing and climate forcing of volcanic eruptions for the
533 past 2,500 years. Nature 523, 543-549.
534 Skinner, L.C., McCave, I.N., 2003. Analysis and modeling of gravity- and piston
535 coring based on soil mechanics. Mar. Geol. 199, 181-204.
536 Steinhilber, F., Beer, J., 2011. Solar activity – the past 1200 years. PAGES News 19,
537 5-6.
538 Tan, L., Cai, Y., Cheng, H., Edwards, R.L., Lan, J., Zhang, H., Li, D., Ma, L., Zhao,
539 P., Gao, Y., 2018. High resolution monsoon precipitation changes on
540 southeastern Tibetan Plateau over the past 2300 years. Quat. Sci. Rev. 195, 122-
541 132. Doi: 10.1016/j.quascirev.2018.07.021
542 Tierney, J.E., Tingley, M.P., 2018. BAYSPLINE: A new calibration for the alkenone
543 paleothermometer. Paleoceanography and Paleoclimatology, 33, 281-301,
544 Wang, Y., Cheng, H., Edwards, R.L., He, Y., Kong, X., An, Z., Wu, J., Kelly, M.J.,
545 Dykoski, C., Li, X., 2005. The Holocene Asian monsoon: links to solar changes
546 and North Atlantic climate. Science 308, 854-857. Doi: 10.1126/science.1106296.
547 Wang, J., Yang, B., Ljungqvist, F.C., Luterbacher, J., Osborn, T.J., Briffa, K.R.,
548 Zorita, E., 2017. Internal and external forcing of multi-decadal Atlantic climate
549 variability over the past 1,200 years. Nat. Geosci. 10, 512-517.
550 Zhang, P., Cheng, H., Edwards, R.L., Chen, F., Wang, Y., Yang, X., Liu, J., Tan, M.,
551 Wang, X., Liu, J., An, C., Dai, Z., Zhou, J., Zhang, D., Jia, J., Jin, L., Johnson,
552 K.R., 2008. A test of climate, sun, and culture relationships from an 1810-year
553 Chinese cave record. Science 322, 940-942.

554 Zhang, H., Griffiths, M.L., Chiang, J.C.H., Kong, W., Wu, S., Atwood, A., Huang, J.,
555 Cheng, H., Ning, Y., Xie, S., 2018. East Asian hydroclimate modulated by the
556 position of the westerlies during Termination I. Science 362, 580-583. doi:
557 10.1126/science.aat9393.
558
559

560 **Figure Captions**
561

562 **Figure 1.** Bi-monthly records of SST and total C_{37} alkenone concentration at the core
563 site. The 12-year averaged SST measured *in situ* was from the NFRDI (2000–2012).
564 Total C_{37} alkenone concentration was measured from suspended surface water
565 particles near the core site for two years (2009–2010) (Lee *et al.*, 2014). The straight
566 line indicates the top core alkenone temperature. The dashed line indicates the annual
567 mean SST. The dashed-dotted line indicates the annual mean SST, considering the
568 weight of the monthly alkenone concentration.
569

570 **Figure 2.** (a) Age-depth model and (b) accumulation rate of the ARA/ES 03-01 GC01
571 core, produced using Bacon 2.2 (Blaauw and Christen, 2011). The asterisk (*)
572 indicates the boundary age of the rapid change in the accumulation rate. The double
573 asterisk (**) indicates the depth and age of the lowest temperature recorded.
574

575 **Figure 3.** Time series of (a) alkenone SST versus calendar year in TY2010 PC4 /
576 ARA/ES 03-01 GC01 cores. The thick line indicates the 10-year averaged alkenone
577 SST. Dashed lines represent intervals of the standard deviation, 1σ. Black triangles
578 indicate radiocarbon dates and their uncertainties. (b) Running standard deviation
579 (100-year window) of the alkenone SST. (c) Tree-ring-based air temperatures in Asia
580 (PAGES 2k Consortium, 2013). The horizontal straight line indicates the mean value
581 for 2k.
582

583 **Figure 4.** Time series of (a) the 40 largest global volcanic aerosol forcings (Sigl *et al.*,
584 2015), (b) alkenone-based SST estimates from TY2010 PC4 / ARA/ES 03-01 GC01
585 cores, (c) total solar irradiance forcing (Roth and Joos, 2013), and (d) greenhouse gas
586 forcing (MacFarling Meure *et al.*, 2006; Joos and Spahni, 2008). Vertical shaded bars
587 indicate grand solar minima (Steinhilber and Beer, 2011). The horizontal dashed line
588 indicates the mean SST value for 2k.
589

590 **Figure 5.** Spectrum analysis of alkenone temperature (this study) and TSI (Roth and
591 Joos, 2013) for the last 2k. Time series of 10-year averaged alkenone temperature
592 were used. For TSI time series, both 1-year resolution (line) and 10-year averaged
593 (dashed line) TSI values were used.
594
595 **Figure 6.** Comparisons of (a) the intensity of volcanic forcing, (b) the number of
596 occurrence of volcanic eruption per 100 years, and (c) the intensity of TSI between
597 two periods (0-1200 CE and 1200-1850). The 32 largest volcanic events for the
598 period of 0-1992 CE (Sigl et al., 2015) were used. TSI data for the last 2k (Roth and
599 Joos, 2013) were used. The box and whiskers denote the upper and lower quartiles,
600 the median, and the minimum and maximum values.
601
602 **Figure 7.** (a) June to October temperature time series of ERSST (Huang *et al*., 2014)
603 and HadISST (Rayner *et al*., 2003) near the core location (130°E, 36°N) and alkenone
604 temperature for the period of 1870-2010 CE, Regression map of HadISST data and
605 alkenone temperature with (b) 11-year running mean temperatures, and (c) detrended
606 temperatures. The HadISST data are from Rayner *et al*. (2003).
607
608 **Figure 8.** Time series of 10-year averaged alkenone temperature of (a) our TY2010
609 PC4 / ARA/ES 03-01 GC01 cores from the western Pacific margin, (b) PCM00-78
610 core from the eastern Pacific margin (Baja California) (O'Mara *et al*., 2019), and (c)
611 running standard deviation (100-year window) of our alkenone temperatures and
612 those of O'Mara et al.(2019). The horizontal line indicates the mean value of each
613 record for 2k. Dashed lines represent intervals of the standard deviation, 1σ.
614
615 **Figure 9.** (a) Rainfall anomalies regressed against instrumental SST (HadISST) at the
616 core site for the period of 1948–2019. The rainfall dataset was obtained from
617 NOAA's PRECipitation REConstruction over Land (PREC/L, Chen et al., 2002). The
618 circles indicate the location of cores and caves. Time series of 10-year averaged (b)

alkenone temperature of our TY2010 PC4 / ARA/ES 03-01 GC01 cores in this study, (c) Wanxiang cave $\delta^{18}O$ (Zhang *et al*., 2008), (d) Shenqi cave $\delta^{18}O$ (Tan *et al*., 2018), (e) Heshang cave $\delta^{18}O$ (Hu *et al*., 2008), and (f) Dongge cave $\delta^{18}O$ (Wang *et al*., 2005). Horizontal lines indicate the mean value of each record for 2k. Dashed lines represent intervals of the standard deviation 1σ.

626 **Table 1** ^{14}C ages for the ARA/ES 03-01 GC01 core
627

Sample Depth (cm)	Material	AMS ^{14}C Age (yr BP)	Calendar Age[a] (CE)	Lab Code[b,c]
40-45	Pl. Foram.	125 ± 20		OS-104642
140-145	Pl. Foram.	535 ± 20	1767 ± 10	OS-104654
250-255	Pl. Foram.	670 ± 25	1619 ± 18	OS-104643
280-285	Pl. Foram.	739 ± 19	1565 ± 19	R40157/1
340-345	Pl. Foram.	820 ± 25	1453 ± 16	OS-104644
380-386	Pl. Foram.	1060 ± 20	1308 ± 16	OS-104645
450-455	Pl. Foram.	1530 ± 25	854 ± 38	OS-104646
540-545	Pl. Foram.	2214 ± 19	145 ± 39	R40157/2

628 [a]Calendar ages were converted from radiocarbon ages using Bacon 2.2 software
629 (Blaauw and Christen, 2011).
630 [b] OS indicates the NOSAMS facility at the WHOI, USA.
631 [c] R indicates the Rafter Radiocarbon Laboratory, New Zealand.
632
633

634 **Table 2** ^{210}Pb and ^{226}Ra activities for the NR2018 BC2 core
635

Core ID	Sample Depth (cm)	Materials	Total ^{210}Pb (mBq/g)[a]	^{226}Ra (mBq/g)[a]	Excess ^{210}Pb (mBq/g)
NR2018 BC2 #1	1-2	Dry sediment	445 ± 13	8.4 ± 2	437
NR2018 BC2 #2	1-2	Dry sediment	487 ± 18	13.8 ± 3	473
NR2018 BC2 #2	10-11	Dry sediment	340 ± 19	11.7 ± 3.3	328
NR2018 BC2 #2	20-21	Dry sediment	290 ± 18	10.6 ± 3.4	279
NR2018 BC2 #2	30-31	Dry sediment	273 ± 15	11.9 ± 3	261
NR2018 BC2 #2	42-43	Dry sediment	197 ± 16	13 ± 3.3	184

636 [a] Total ^{210}Pb and ^{226}Ra activities were measured at the at the Korea Basic Science
637 Institute.
638

639 **Table 3** Correlation coefficents between the reconstructed SST and TSI

640

	Reconstructed SST & TSI*			
Period	140-2000	1200-2000	1500-2000	1600-2000
Correlation Coefficent	0.17**	0.23**	0.27**	0.54***

641 *: The TSI data are from Roth and Joos (2013).

642 **: 95% confidence level

643 ***: 99% confidence level

Fig. 1
Lee et al.

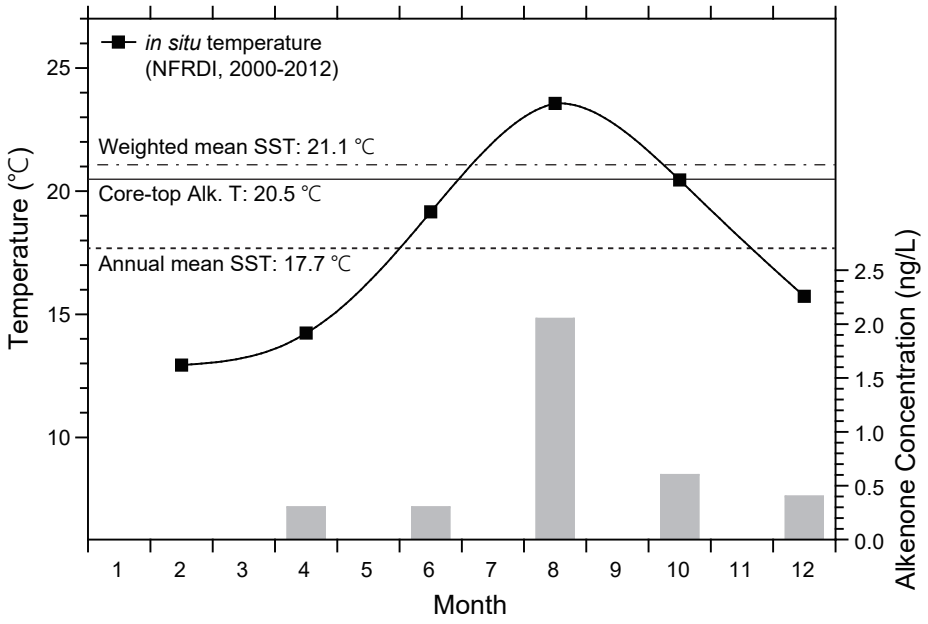

Fig. 2
Lee et al.

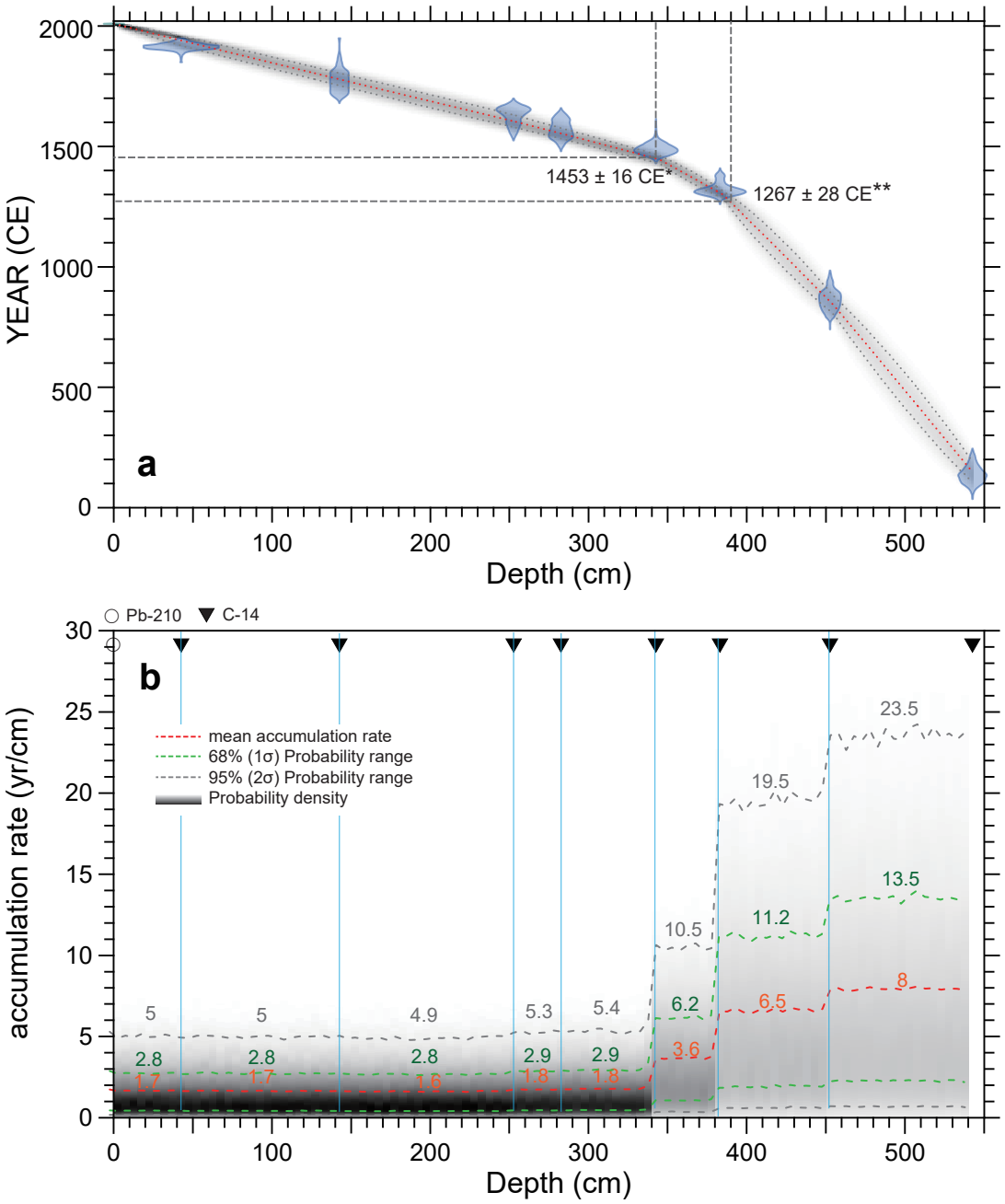

Fig. 3
Lee et al.

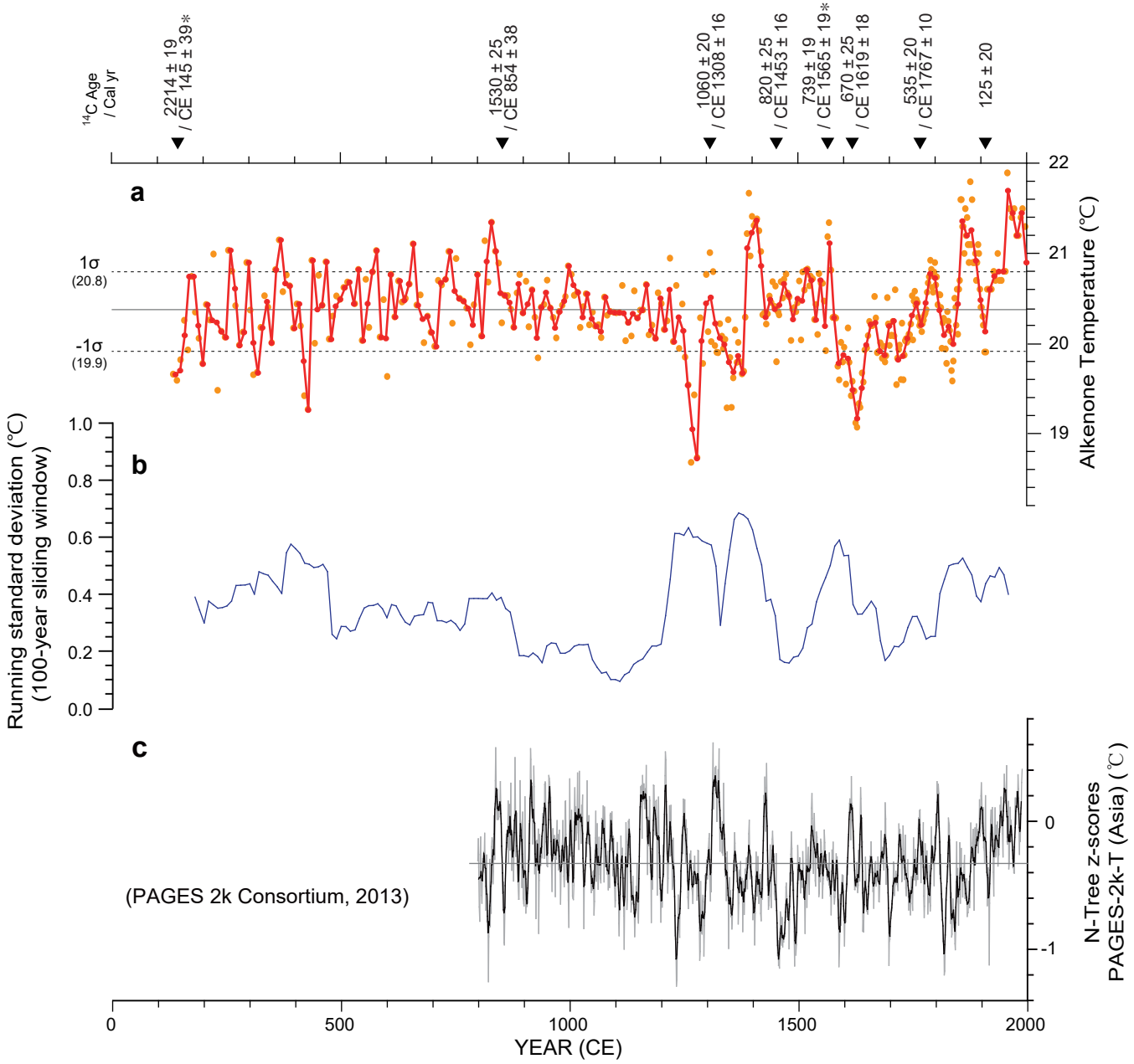

Fig. 4
Lee et al.

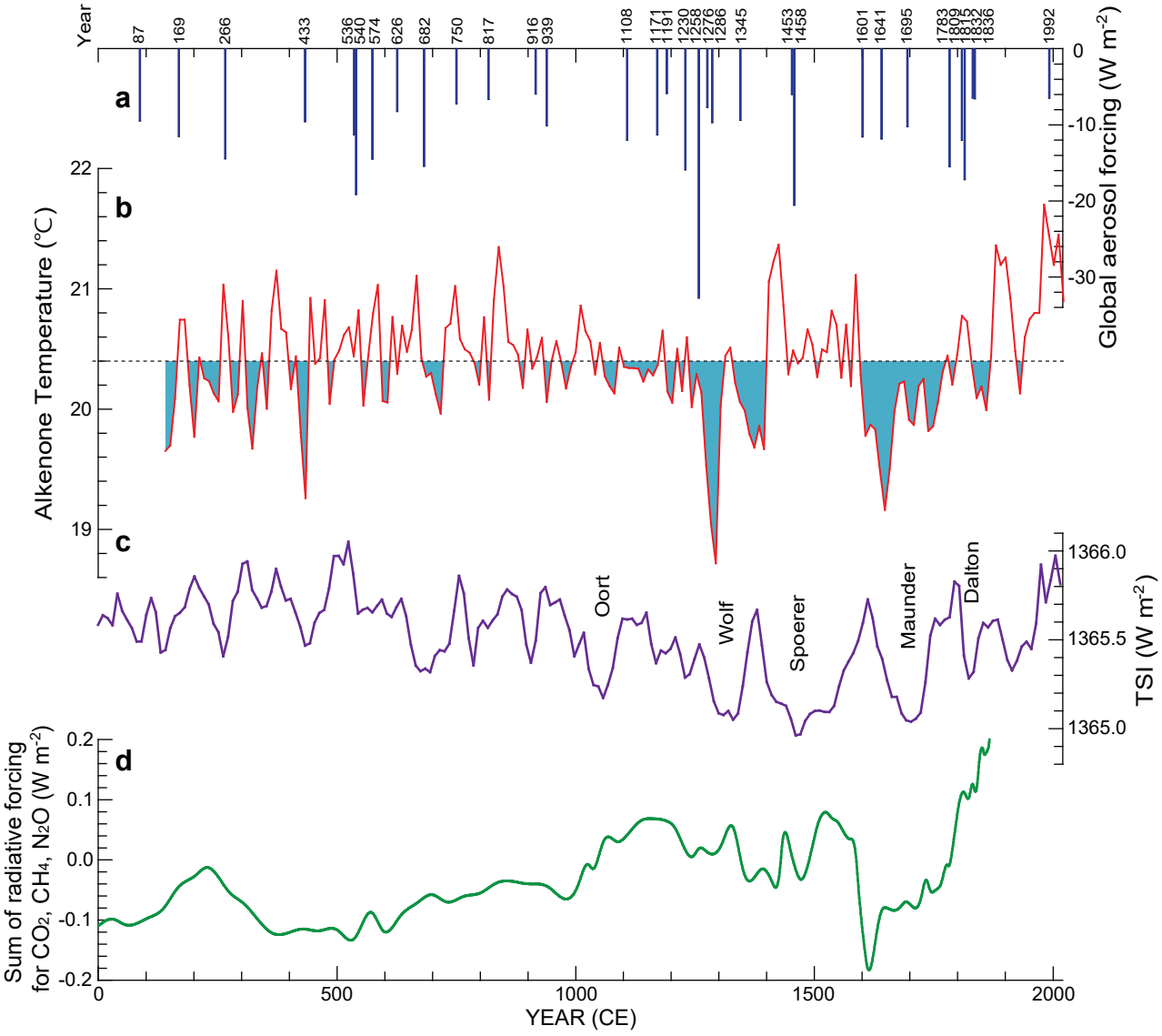

Fig. 5
Lee et al.

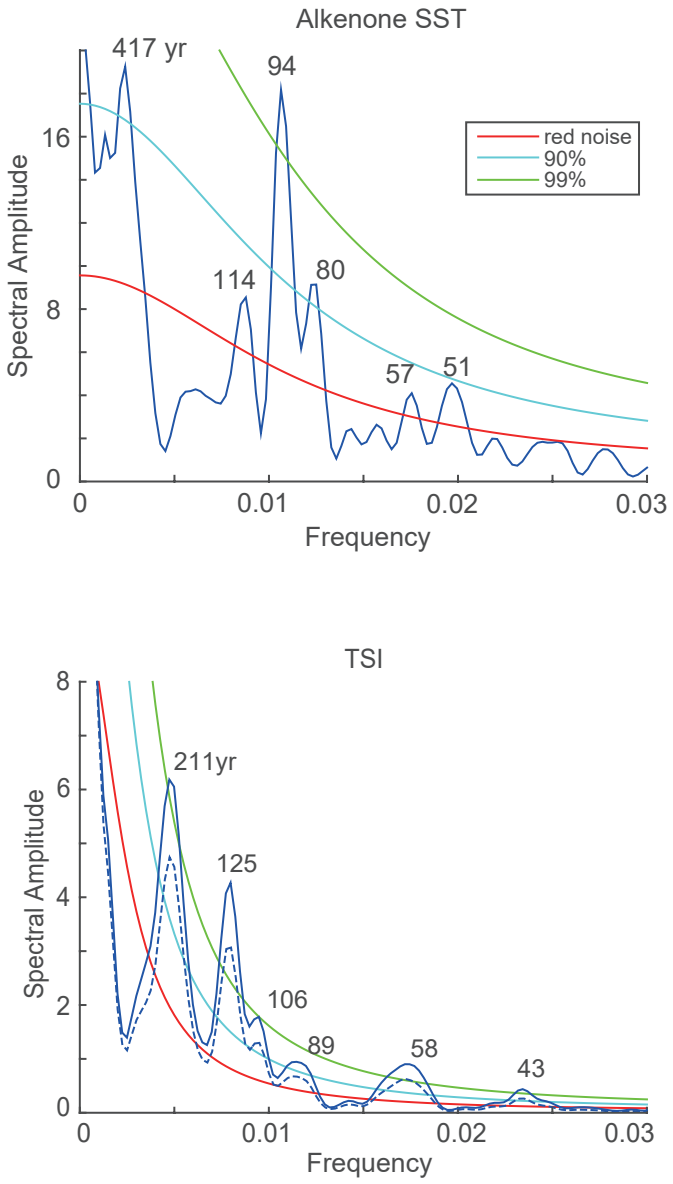

Fig. 6
Lee et al.

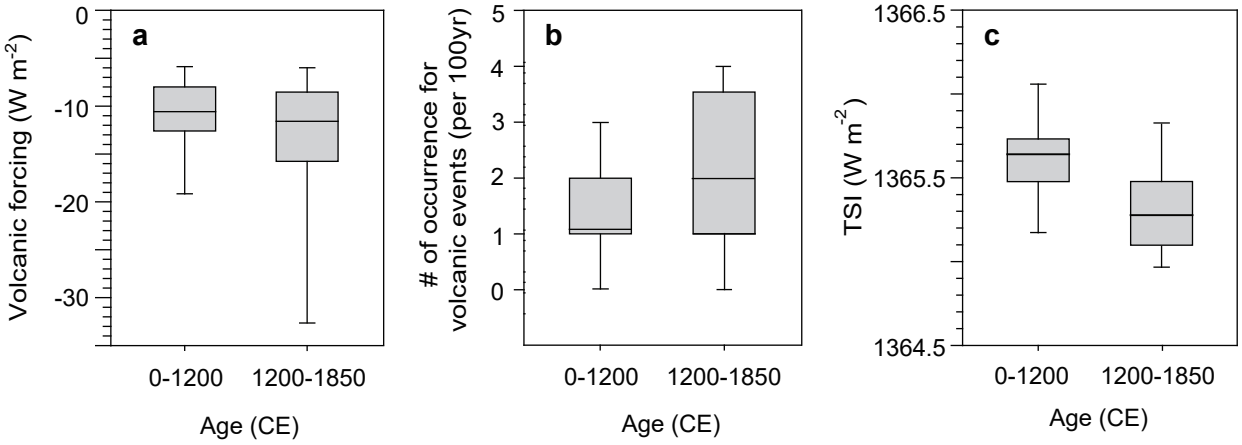

Fig. 7
Lee et al.

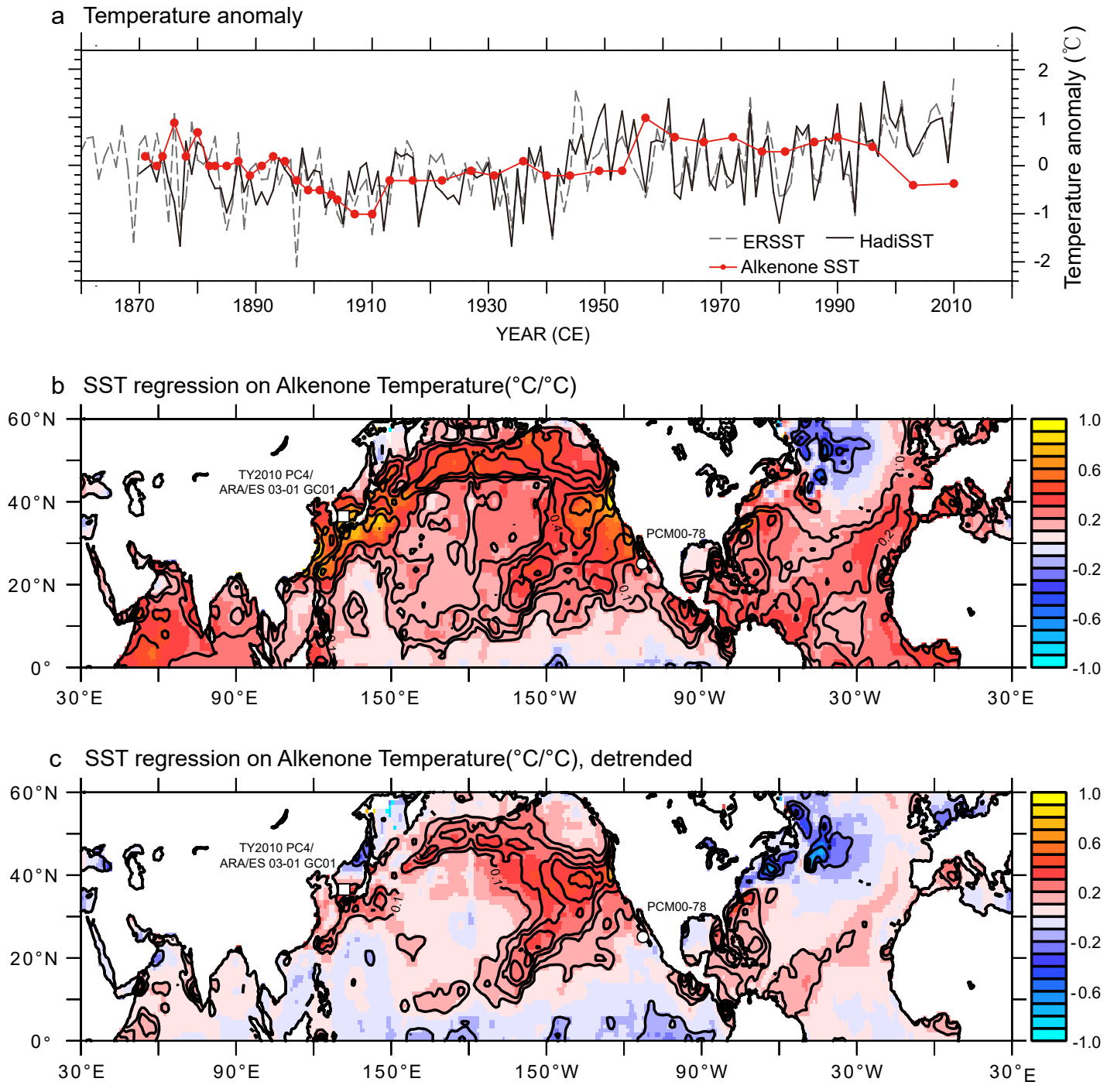

Fig. 8
Lee et al.

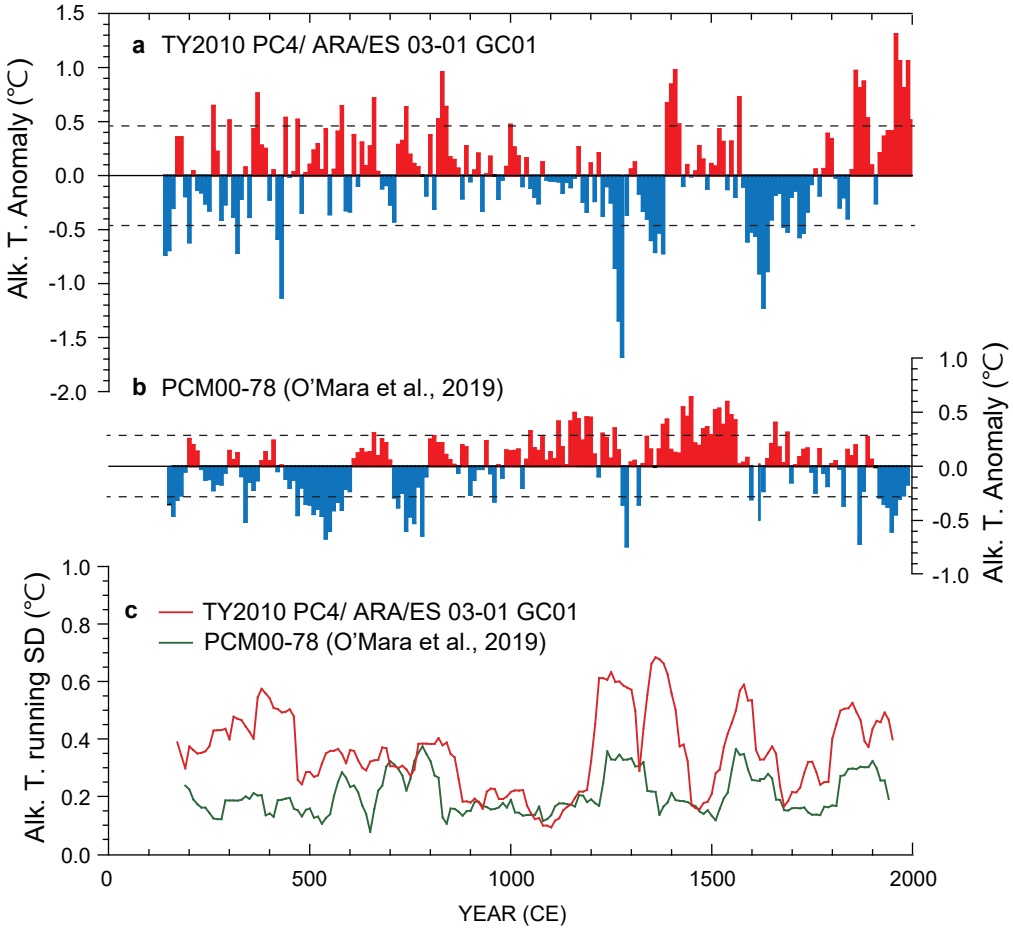

Fig. 9
Lee et al.